We are IntechOpen, the world's leading publisher of Open Access books Built by scientists, for scientists

4,800
Open access books available

122,000
International authors and editors

135M
Downloads

Our authors are among the

154
Countries delivered to

TOP 1%
most cited scientists

12.2%
Contributors from top 500 universities

CLARIVATE ANALYTICS BOOK CITATION INDEX INDEXED

WEB OF SCIENCE™

Selection of our books indexed in the Book Citation Index in Web of Science™ Core Collection (BKCI)

Interested in publishing with us?
Contact book.department@intechopen.com

Numbers displayed above are based on latest data collected.
For more information visit www.intechopen.com

25

Conjugate Flow and Heat Transfer of Turbine Cascades

Jun Zeng and Xiongjie Qing
China Gas Turbine Establishment
P. R. China

1. Introduction

Heat transfer design of HPT airfoils is a challenging work. HPT usually requires much cooling air to guarantee its life and durability, but that will affect thermal efficiency of turbine and fuel consumption of engine[1]. The amount of blade cooling air depends on the prediction accuracy of temperature field around turbine airfoil surface, which is related to the prediction accuracy of temperature field in laminar-turbulent transition region. The laminar-turbulent transition is very important in modern turbine design. On suction side of turbine airfoil, the flow is relaminarized under the significant negative pressure gradient. In succession, when the relaminarized flow meets enough large positive pressure gradient, laminar-turbulent transition appears. In transition region, the mechanisms of flow and heat transfer are complicated, so it is hard to simulate the region.

Methods of conjugate flow and heat transfer analysis have been discussed extensively. In 1995, Bohn[2] simulated the heat transfer along Mark II[3] cascade using a two-dimensional (2D) conjugate method at the transonic condition (the exit isentropic Mach number is 1.04). In his simulation, the turbulence model used was Baldwin-Lomax model. The result was that the max difference between the predicted temperature along the cascade and the test data was not larger than 15K. The method was also used to simulate C3X[3] turbine cascade at 2D boundary conditions by Bohn[4], and a good agreement between the prediction results and the test data was gotten. Bohn also published a paper[5] in which Mark II turbine cascade with thermal barrier coatings was calculated in 2D cases. The ZrO_2 coatings with a thickness of 0.125mm bonded a 0.06mm MCrA1Y layer were applied. There were two configurations of the coatings. The problems and the influence of coatings on the thermal efficiency were solved by the same solver and evaluated. On the basis, the 3D numerical investigation of conjugate flow and heat transfer about Mark II with thermal barrier coating was done[6]. The uncoated vane was also used to validate the 3D method. The influence of the reduced cooling fluid mass flow on the thermal stresses was discussed in detail. York[7] used 3D conjugate method to simulate C3X turbine cascade. Because no transition model was used, the simulated external HTC (EHTC) at the leading edge stagnation point and laminar region had low precision. Facchini[8] made another 3D conjugate heat transfer simulation of C3X, however there was an obvious difference of HTC between simulation results and experimental data. Sheng[9] researched 3D conjugate flow and heat transfer

method of turbine. In some reference, the effect of transition on conjugate flow and heat transfer was not mentioned.

Because of laminar-turbulent transition on suction side of turbine airfoil and the transition consequentially effects conjugate flow and heat transfer, high precision transition models must be researched.

The best method for the simulation of conjugate flow and heat transfer case is Large Eddy Simulation (LES) or Direct Numerical Simulations (DNS). The two methods have high accuracy of predicting flow and heat transfer in transition region, but they are not suitable for engineering application nowadays, because they are too costly. At present, the better method for conjugate simulation is still using two-equation turbulence model with transition model.

In this paper, the numerical method considering transition was used to predict 2D and 3D conjugate flow and heat transfer. T3A flat plate, VKI HPT stator, VKI HPT rotor and MARK II stator were calculated. T3A flat plate was used to validate the accuracy of aerodynamic simulation, and the conjugate flow and heat transfer cases of other blades were calculated to validate the method. In the conjugate simulations, the effect of various turbulence models and inlet turbulence intensities on heat transfer were investigated.

2. Numerical method

2.1 Governing equations

The governing equations were:

Continuity equations:

$$\frac{\partial \rho}{\partial t}+\frac{\partial \rho U_i}{\partial x_i}=0$$

Momentum equations (N-S equations):

$$\frac{\partial \rho U_i}{\partial t}+\frac{\partial \rho U_i U_j}{\partial x_j}=-\frac{\partial p}{\partial x_i}+\frac{\partial}{\partial x_j}\left(\mu_{eff}\left(\frac{\partial U_i}{\partial x_j}+\frac{\partial U_j}{\partial x_i}\right)\right)-\frac{2}{3}\frac{\partial}{\partial x_i}\left(\mu_{eff}\frac{\partial U_j}{\partial x_j}\right)$$

Energy equations:

$$\frac{\partial \rho h^*}{\partial t}+\frac{\partial \rho U_i h^*}{\partial x_i}=\frac{\partial p}{\partial t}+\frac{\partial}{\partial x_i}\left(\lambda\frac{\partial T}{\partial x_i}\right)+\frac{\partial}{\partial x_j}\left(\mu_{eff}U_i\left(\frac{\partial U_i}{\partial x_j}+\frac{\partial U_j}{\partial x_i}\right)\right)-\frac{2}{3}\frac{\partial}{\partial x_i}\left(\mu_{eff}U_i\frac{\partial U_j}{\partial x_j}\right)$$

For thermal conduction of solid, when there is no thermal source, the governing equations were:

$$\frac{\partial \rho c T}{\partial t}=\frac{\partial}{\partial x_i}\left(\lambda\frac{\partial T}{\partial x_i}\right)$$

On the interface of fluid and solid, heat flux is equivalent.

The governing equations were discretized with finite volume method. By means of solving continuity equations and Momentum equations simultaneously, the uncoupling of pressure and temperature was resolved. Convection term has second-order precision.

2.2 Turbulence model

Advanced turbulence model with high accuracy of describing turbulence nature must be used to get exact flow field, especially for engineering problems. In order to improve accuracy of flow and heat transfer analysis, Menter[10] developed SST turbulence model. The model assimilated the advantages of k-ω model and k-ε model. It used k-ω model near wall and k-ε model far from wall, having high accuracy of predicting flow field near wall and avoiding strong sensitivity to free stream conditions. A number of test cases were predicted by means of the model, proving that the model has high accuracy of conjugate flow and heat transfer problem especially for large adverse pressure gradient[11].

2.3 Transition model

Transition has significant effect on heat transfer. In order to predict conjugate flow and heat transfer of turbine cascades, turbulence model must be coupled with transition model. Experience modified transition models include zero-equation model, one-equation model and two-equation model. Intermittency is given in zero-equation model. In one-equation model, user-defined transition Reynolds number is used to solve intermittency, avoiding solving another equation so that reduce computation time, but the model does not consider effect of turbulence intensity and pressure gradient on transition. Two-equation model connects free stream turbulence intensity with transition momentum thickness Reynolds number at the onset of transition and solves two transport equations. One is used to calculate intermittency and the other is used to calculate momentum thickness Reynolds number. The two equations couple with production terms in SST turbulence model. The two-equation model can solve the transition caused by shock wave or separation. In order to predict complex cascade flow field with high accuracy and improve the solving precision of temperature and external heat transfer coefficient along airfoils, the modified two-equation transition model developed by Menter[12] was used.

The transport equation of intermittency γ in the two-equation transition model is:

$$\frac{\partial(\rho\gamma)}{\partial \mathrm{t}}+\frac{\partial(\rho U_j\gamma)}{\partial x_j}=P_{\gamma 1}-E_{\gamma 1}+P_{\gamma 2}-E_{\gamma 2}+\frac{\partial}{\partial x_j}\left((\mu+\mu_t)\frac{\partial\gamma}{\partial x_j}\right)$$

where:

$$P_{\gamma 1}=2F_{length}\rho S(\gamma F_{onset})^{0.5}\ ;\ E_{\gamma 1}=P_{\gamma 1}\gamma\ ;$$

$$P_{\gamma 2}=0.06\rho\Omega\gamma F_{turb}\ ;\ E_{\gamma 2}=50P_{\gamma 2}\gamma\ ;$$

$$F_{onset}=\max\left(F_{onset2}-F_{onset3},0\right)\ ;\ F_{turb}=e^{-(0.25R_T)^4}\ ;$$

$$F_{onset1}=\frac{\mathrm{Re}_v}{2.193\mathrm{Re}_{\theta c}}\ ;\ F_{onset2}=\min\left(\max\left(F_{onset1},F_{onset1}^4\right),2.0\right);\ F_{onset3}=\max\left(1-\left(\frac{R_T}{2.5}\right)^3,0\right);$$

$$\mathrm{Re}_v=\frac{\rho y^2 S}{\mu}\ ;\ R_T=\frac{\rho k}{\mu\omega}\ ;\ S=\sqrt{2S_{ij}S_{ij}}\ ;\ \Omega=\sqrt{2\Omega_{ij}\Omega_{ij}}\ ;\ S_{ij}=\frac{1}{2}\left(\frac{\partial U_i}{\partial x_j}+\frac{\partial U_j}{\partial x_i}\right);\ \Omega_{ij}=\frac{1}{2}\left(\frac{\partial U_i}{\partial x_j}-\frac{\partial U_j}{\partial x_i}\right)$$

For the transition caused by separation, the correction is:

$$\gamma_{eff} = \max\left(\gamma, \gamma_{sep}\right)$$

where:

$$\gamma_{sep} = \min\left(2 \bullet \max\left(\left(\frac{\mathrm{Re}_v}{3.235\mathrm{Re}_{\theta c}}\right) - 1, 0\right) F_{reattach}, 2\right) F_{\theta t};\ F_{reattach} = e^{-\left(\frac{R_T}{20}\right)^4};$$

The transport equation of transition momentum thickness Reynolds number $\tilde{\mathrm{Re}}_{\theta t}$ in the two-equation transition model is:

$$\frac{\partial(\rho \tilde{\mathrm{Re}}_{\theta t})}{\partial \mathrm{t}} + \frac{\partial(\rho U_j \tilde{\mathrm{Re}}_{\theta t})}{\partial x_j} = P_{\theta t} + \frac{\partial}{\partial x_j}\left(2 \bullet (\mu + \mu_t)\frac{\partial \tilde{\mathrm{Re}}_{\theta t}}{\partial x_j}\right)$$

where:

$$P_{\theta t} = 0.03\frac{\rho}{t_1}\left(\mathrm{Re}_{\theta t} - \tilde{\mathrm{Re}}_{\theta t}\right)\left(1 - F_{\theta t}\right);\ t_1 = \frac{500\mu}{\rho U^2};$$

$$F_{\theta t} = \min\left(\max\left(F_{wake} \bullet e^{-\left(\frac{y}{\delta}\right)^4}, 1 - \left(\frac{\gamma - 0.02}{1 - 0.02}\right)^2\right), 1\right)$$

$$\delta = \frac{50\Omega y}{U} \bullet \delta_{BL};\ \delta_{BL} = 7.5\theta_{BL};\ \theta_{BL} = \frac{\tilde{\mathrm{Re}}_{\theta t}\mu}{\rho U};$$

$$F_{wake} = e^{-\left(\frac{\mathrm{Re}_\omega}{1\times10^5}\right)^2};\ \mathrm{Re}_\omega = \frac{\rho\omega y^2}{\mu};$$

$\mathrm{Re}_{\theta t}$ is the transition momentum thickness Reynolds number in experiment.

3. Validation

3.1 T3A flat plate

The geometric configuration and the boundary conditions of ERCOFTAC T3A[13] flat plate were shown in figure 1. The case was used to validate SST turbulence model with transition.

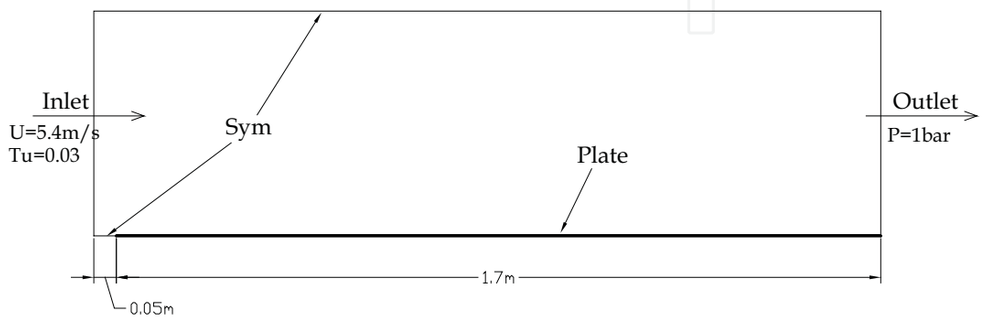

Fig. 1. Geometric configuration and boundary conditions of T3A

The computational mesh was shown in figure 2. Near the leading edge of T3A, the mesh density is the largest. The mesh included both tetrahedral and prismatic mesh. Total number of nodes was 67538 and total number of elements was 115090.

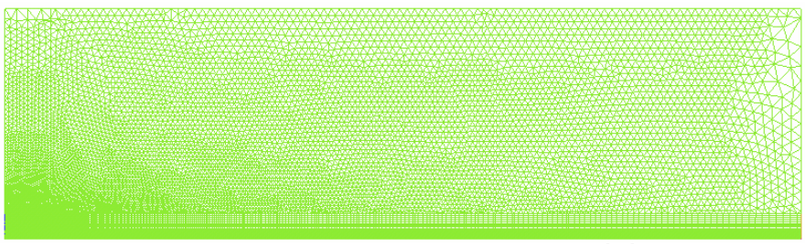

Fig. 2. Tetrahedral mesh of T3A

Figure 3 showed comparison between skin friction coefficient of predicted result and the one of test. It was shown that SST turbulence model with transition model ("transition" in the figure) has high accuracy of predicting the onset of transition in flat plate case. Around the leading edge of the plate, flow is laminar. In this region, SST model without transition model ("fully turbulent" in the figure) over predicted the friction coefficient. In the region of fully turbulent flow, the effect of transition model on friction coefficient is insignificant.

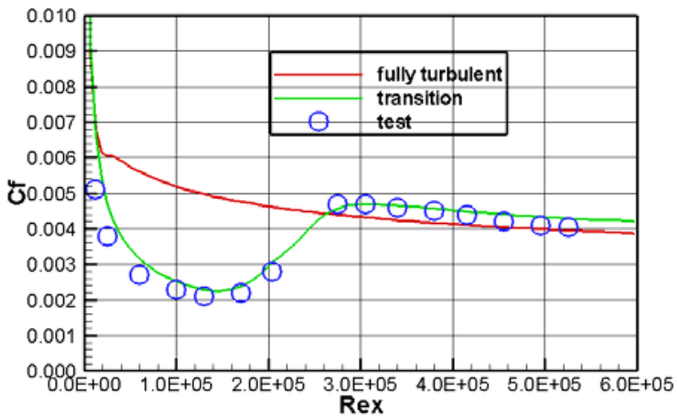

Fig. 3. Skin friction coefficient of T3A

The influence of the mesh shape on the simulation was also researched. A mesh only including hexahedral elements was created, as shown in figure 4. Total number of nodes was 123328 and total number of elements was 91233.

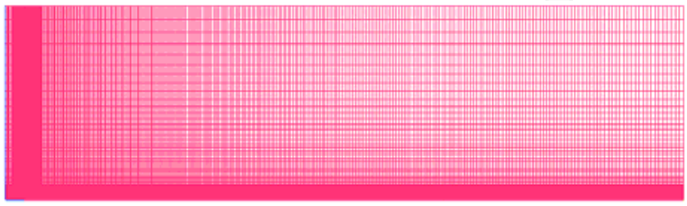

Fig. 4. Hexahedral mesh of T3A

Figure 5 showed the simulation results by means of hexahedral mesh. The result with transition model was also in good agreement with the test data. The trend of the predicted

skin friction with transition model was similar to the result of the tetrahedral mesh. Figure 5b imply that the mesh shape had insignificant influence on the results.

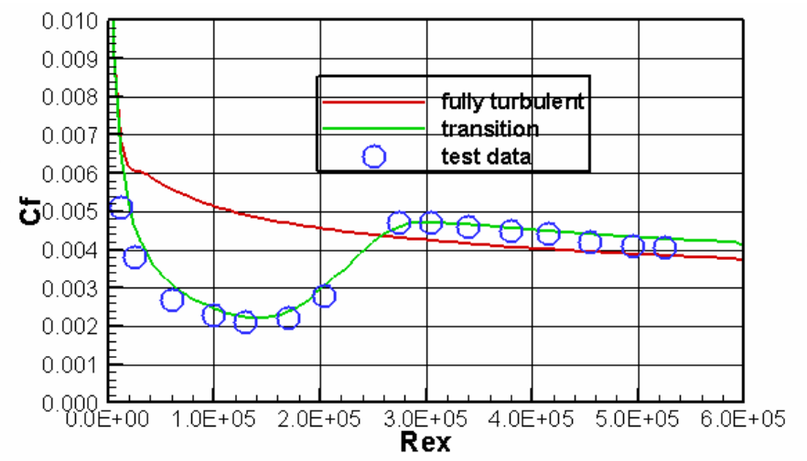

a) Simulation results

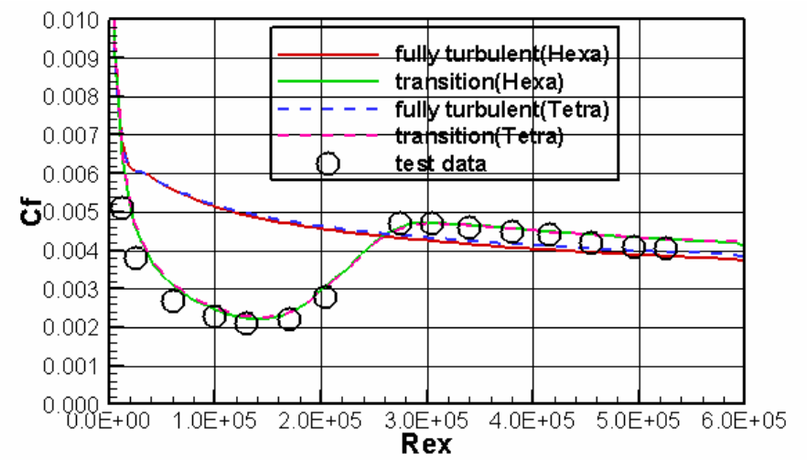

b) Compared to tetrahedral mesh

Fig. 5. Skin friction coefficient of T3A with hexahedral mesh

3.2 VKI HPT stator

VKI HPT stator was shown in figure 6. The geometric data was also given in the figure, and detail geometric data could be found in the reference 14. The computational mesh (in figure 7) was hexahedron. Total number of nodes was 109272. Altogether two predictions were made, and the boundary conditions were shown in table 1.

Condition	Tu	M_{2is}	Re_2	P_1^* /bar	T_1^* /K	P_2 /bar	T_w /K
1	1%	0.92	5×10^5	0.803	420	0.464	300
2	1%	0.92	2×10^6	3.21	420	1.86	300

Table 1. Boundary conditions of the cascade

Geometric data	
Chord/mm	67.647
Pitch/mm	57.500
Stagger Angle/°	55.0
Throat/mm	17.568
Leading edge thickness/mm	8.252
Trailing edge thickness/mm	1.420

Fig. 6. Sketch and geometric data of VKI stator cascade

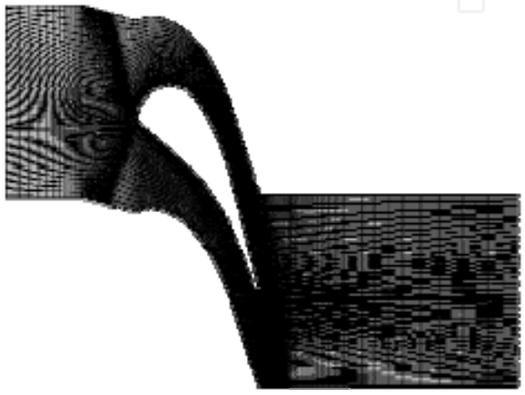

Fig. 7. Computational mesh of VKI stator cascade

Figure 8 showed the results at condition 1. On suction side of the airfoil, a large adverse pressure gradient was found near the trailing edge. The pressure gradient resulted in flow separation, inducing laminar-turbulent transition. The predicted onset of transition was closer to trailing edge as compared to the test data.

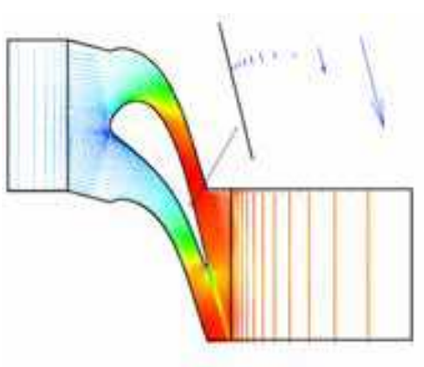

a) Velocity vector

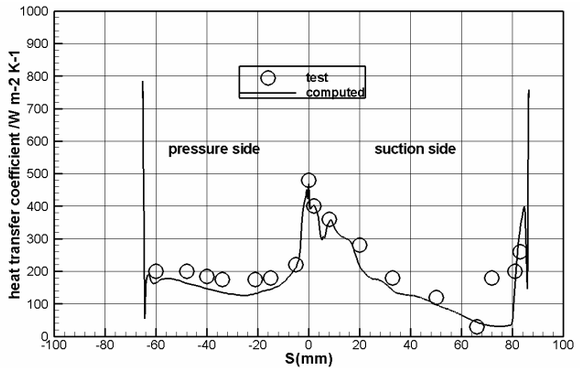

b) EHTC distribution

Fig. 8. Results at condition 1

Figure 9 showed the EHTC distribution of the cascade at condition 2. In the most regions, the predicted EHTC agreed with the test one. The onset of transition was downstream predicted and the transition was predicted more sharply than test. In the low turbulence intensity, the method has high accuracy of predicting EHTC with various Reynolds number.

Comparing figure 8 with figure 9, it can be seen that EHTC increased with Reynolds number increment when other conditions were equivalent.

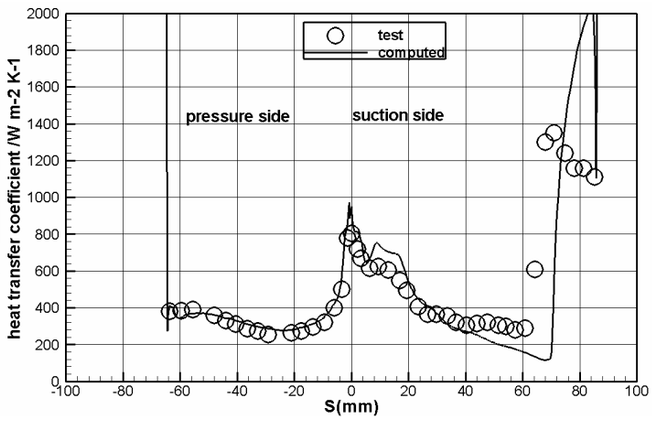

Fig. 9. EHTC distribution at condition 2

3.3 VKI HPT rotor

VKI HPT rotor was shown in figure 10. The geometric data was also given in the figure, and detail geometric data could be found in the reference 15. The hexahedral computational mesh was shown in figure 11. Total number of nodes was 39042. According to various turbulence intensities, two predictions were made.. The boundary conditions were shown in table 2.

Geometric data	
Chord/mm	69.84
Pitch/mm	59.84
Inlet angle/^{o}	40.0
Trailing edge thickness/mm	1.4

Fig. 10. Sketch and Geometric data of VKI rotor cascade

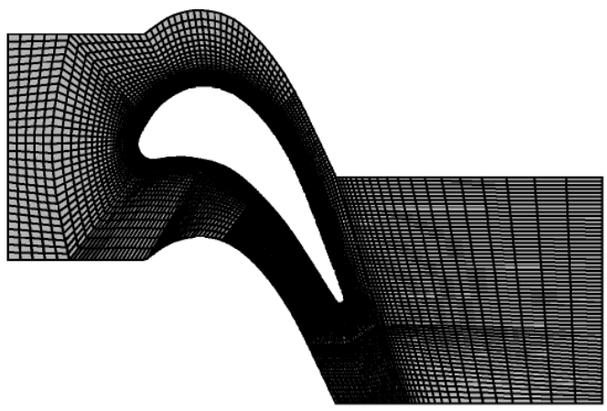

Fig. 11. Computational grid of VKI rotor cascade

condition	Tu	M_{2is}	Re_2	P_1^* /bar	T_1^* /K	P_2 /bar	T_w /K
1	1%	0.92	5×10^5	0.803	420	0.464	300
2	4%	0.92	5×10^5	0.803	420	0.464	300

Table 2. Boundary conditions of the cascade

Figure 12 showed the comparison between the predicted EHTC and the test data at the two conditions. For the onset of transition, the predicted one agreed with the test one at condition 1, and the predicted one was upstream of the test one at condition 2. Under the two turbulence intensities, the predicted EHTC in the laminar region located on suction side agreed with the test one. On pressure side, the predicted EHTC agreed well with the test one when intensity was 1%, and the predicted one was lower than the test one when intensity was 4%. The method has high accuracy of predicting EHTC under low turbulence intensity. That intensity increment resulted in EHTC growth.

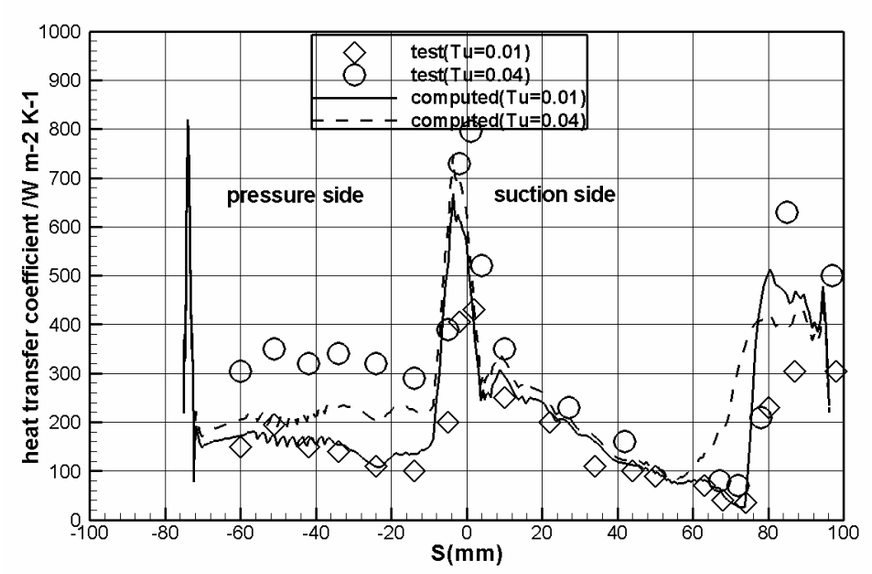

Fig. 12. EHTC distribution (condition 1 and 2)

4. Mark II stator

Mark II HPT stator is convectively cooled by ten cooling channels. The cooling medium is air. The geometric data and cooling channels were shown in figure 13. The detail geometric data could be found in the reference 3. The material of the stator is ASTM 310 stainless steel, the density of which is 7900 kg m^{-3} and the specific pressure heat capacity is 586.5 J kg^{-1} K^{-1}. The thermal conductivity varies as temperature changes, the function is:

$$\lambda = 6.811 + 0.020176 \bullet T$$

Hylton L. D[3] researched the airfoil with experiment method, and got detail aerodynamic and thermal test data. Consequently MARK II stator becomes a typical case for conjugate flow and heat transfer simulations, which is applied to validating codes or the accuracy of methods.

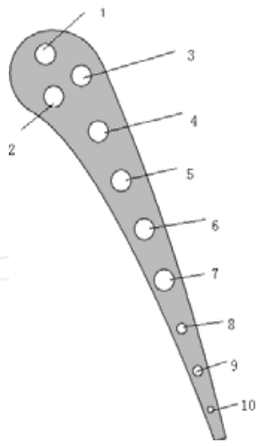

Geometric data	
Chord/mm	136.22
Pitch/mm	129.74
Height/mm	76.2
Stagger angle/◦	63.69
Throat/mm	39.83
Leading edge thickness/mm	12.80

Fig. 13. Sketch and geometric data of MARK Ⅱ cascade

4.1 2D simulation

The 2D simulation used unstructured grid (shown in figure 14), increasing the grid density around wall in the fluid domain and the solid domain. Total number of nodes was 35279 and total number of elements was 58618. Total number of nodes in the fluid domain was 23143 and total number of elements in the fluid domain was 38158. Total number of nodes in the solid domain was 12136 and total number of elements in the solid domain was 20460. The boundary conditions were shown in table 3. The boundary conditions of cooling channel were given cooling temperature and heat transfer coefficient. All boundary conditions could be seen in the reference 3.

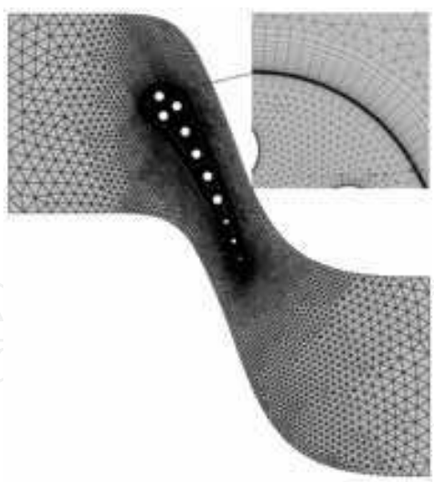

Fig. 14. Computational grid of MARK Ⅱ cascade

Condition	Tu	M_{2is}	Re_2	P_1^* /bar	T_1^* /K	P_2 /bar
1	6.5%	0.89	1.98×10^6	3.44	784	2.08
2	6.5%	1.04	2.01×10^6	3.39	788	1.73

Table 2. Boundary conditions of MARK II cascade

4.1.1 The simulation result of SST with transition model

Figure 15 showed the pressure distributions at subsonic (condition 1) and transonic (condition 2) conditions by using SST with transition model. Along the entire surface of the cascade, the predicted pressure distribution agreed with the test results. In the most regions on pressure side, the distributions of the two conditions were the same, and had no relationship with exit pressure. On suction side, from the location of stagnation point to the location of the first shock wave, a large negative pressure gradient made flow relaminarized. In the next region, shock wave appeared, resulting in laminar-turbulent transition, and the flow finally became turbulent. At the subsonic condition, the predicted onset of the shock wave was slightly on the upstream of that at the transonic condition. However, at the subsonic condition, the intersection of the shock wave and boundary layer resulted in separation. In the laminar regions under the two conditions, the various exit pressures had no effect on surface pressure. In the region downstream of shock wave, the surface pressure distributions at the two conditions differed from each other. At the subsonic conditions, after shock wave, flow accelerated slowly and then decelerated until flow arriving in the trailing edge. At the transonic conditions, after shock wave, flow straightly accelerated to the trailing edge until trailing shock wave was met.

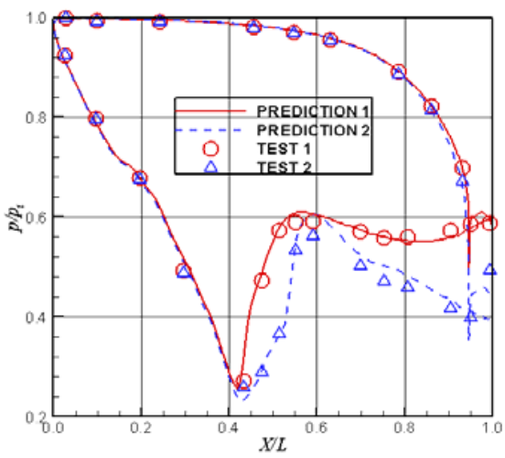

Fig. 15. Pressure distributions (condition 1 and 2)

Figure 16 showed Mach number contour and temperature contour at the subsonic and transonic conditions. At the subsonic condition, separation appeared at the location of 0.43 axial chord on suction side. At the transonic condition, there was no separation in the same location and shock wave appeared at the trailing edge. Upstream of the trailing edge on pressure side, flow accelerated fast resulting in gas temperature reduced rapidly in the solid domain, temperature was kept at a low level because of cooling air in cooling channels, the minimum value of which appeared between cooling channel 2 and cooling channel 3, and the maximum value of which appeared at the trailing edge.

Figure 17 demonstrated surface temperature distributions at the two conditions. The predicted distribution trend agreed with the test data, and the predicted distributions agreed with the test data in most regions. At the stagnation point and the laminar region on suction side, the predicted temperature had high accuracy at the two conditions. On the suction, shock wave appeared resulting in laminar-turbulent transition. Strong heat transfer made temperature curve becoming abrupt in the region of transition, and the maximum

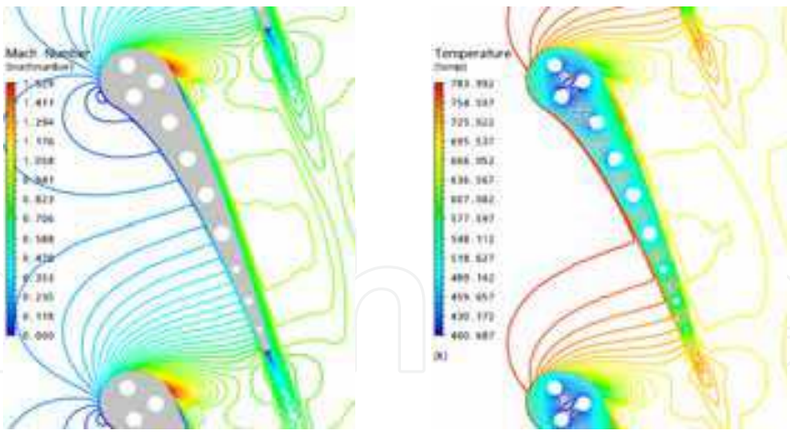

a) condition 1

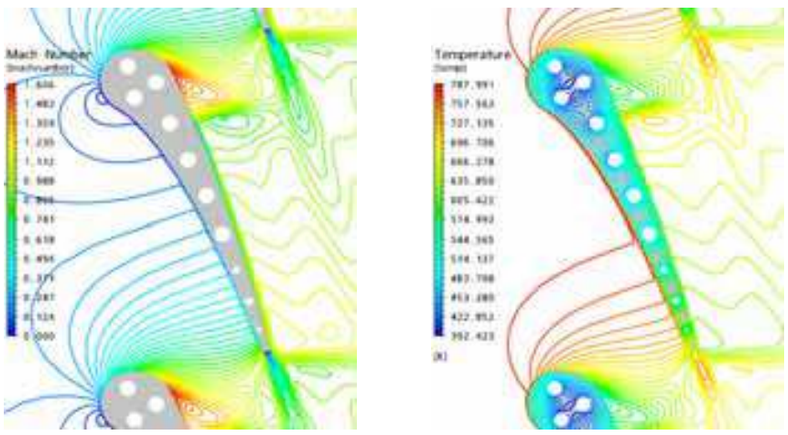

b) condition 2

Fig. 16. Contours of Mach Number and Temperature (condition 1 and 2)

appeared at the end of the transition region. The numerical method over predicted the maximum temperature, especially at the subsonic condition, and the difference between the maximum temperature and the test data was 30K. In the fully turbulent region, the difference between the predicted temperature and the test data became smaller. On entire pressure side, the predicted temperature agreed with the test results. On pressure side and suction side, temperature distribution fluctuated, and the maximum and minimum values appeared in some locations. The minimum values located around cooling channels and the maximum value located between two channels. The maximum temperature on the entire surface located in the trailing edge. The EHTC was high at this location and the channel 10 was far from the location, so that the air could not effectively cool the trailing edge.

EHTC distribution along the airfoil at two conditions was shown in figure 18. As same as the temperature distribution, in the laminar region of suction side and the one of pressure side, the predicted EHTC agreed with the test data. Consequently the method predicted the onset of transition accurately. In transition region, EHTC increased abruptly and encountered the maximum at the end of the transition region where the method over predicted the EHTC. In the turbulent region downstream the transition one, the difference between the predicted EHTC and the test one reduced gradually.

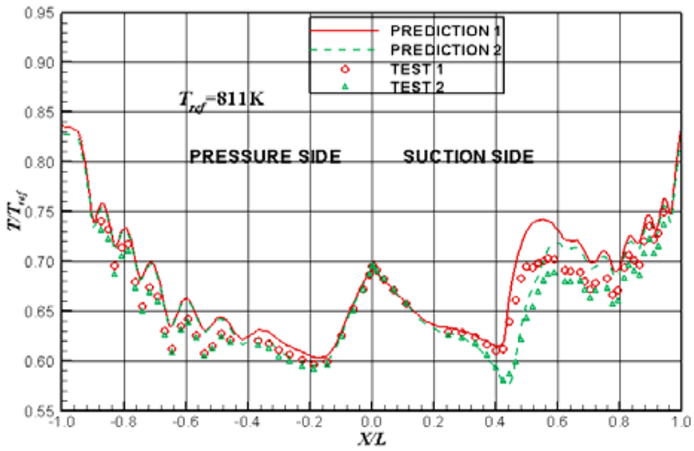

Fig. 17. Temperature distribution (condition 1 and 2)

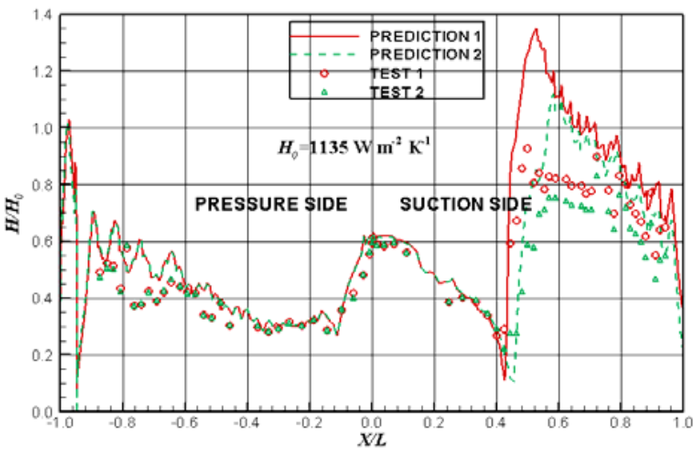

Fig. 18. EHTC distribution (condition 1 and 2)

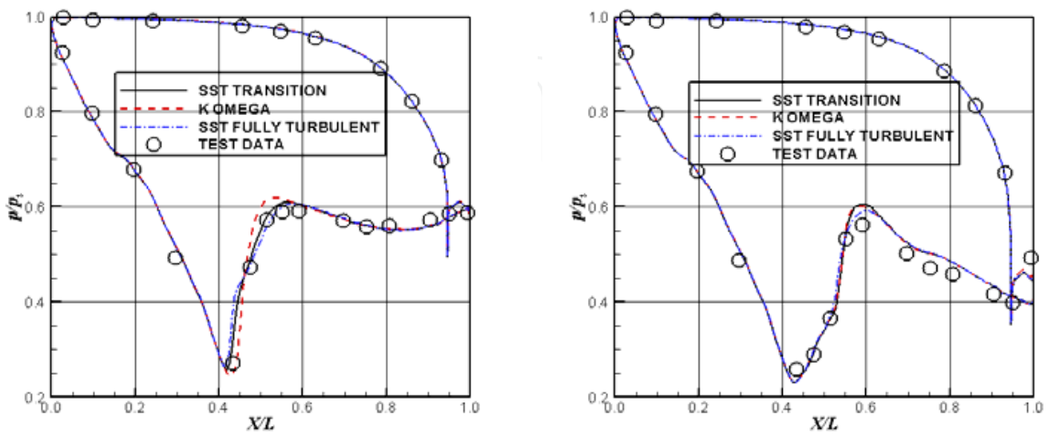

a) Condition 1 b) Condition 2

Fig. 19. Pressure distribution of different turbulence models

4.1.2 The effect of turbulence models

Figure 19 showed the surface pressure distributions of simulations by using k-ω turbulence model (model 1), SST model with fully turbulent flow (model 2) and SST turbulent model with transition model (model 3) at the two conditions. Except around shock wave, the pressure distributions using the three models agreed with each other. At the subsonic condition, the predicted pressure distributions around shock wave by means of model 2 and model 3 agreed with the test data, and the predicted intensity of shock wave by means of model 1 was stronger than the test results. At the transonic condition, the predicted pressure distribution using model 2 was closest to the test data. However, as a whole, the three models had high accuracy of predicting surface pressure distributions.

Figure 20 showed EHTC distributions of the three models. Whether subsonic or transonic condition, the predicted EHTC by means of model 1 or model 2 at the stagnation point and in the laminar region had large difference from the test data. In the regions, the predicted results by means of model 3 agreed with the test data. In the fully turbulent region, the results of the three models were close to each other, agreeing with the test data.

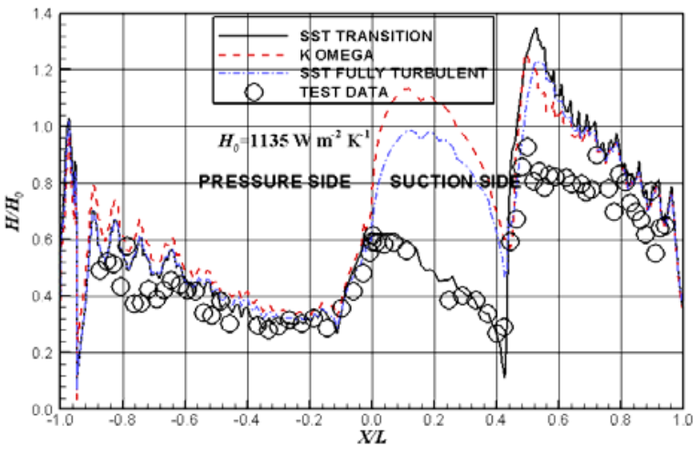

a) Condition 1

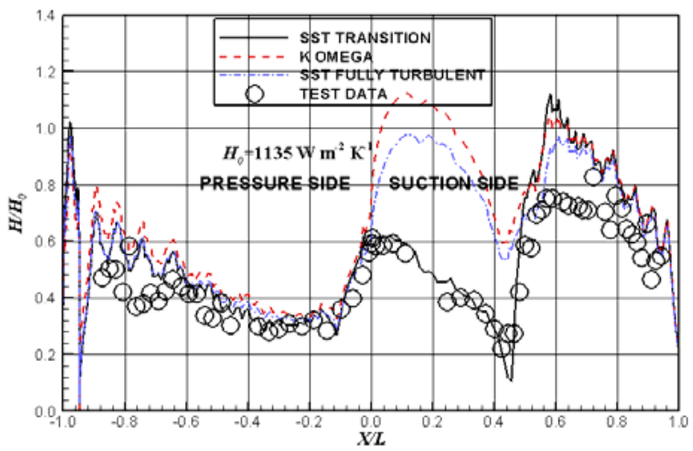

b) Condition 2

Fig. 20. EHTC distributions of different turbulence models

4.1.3 The effect of inlet turbulence intensities

Model 3 was used to research the effect of inlet turbulence intensities on predicted surface pressure and temperature. Figure 21 illustrated surface pressure distributions with various inlet turbulence intensities at the two conditions. Whether subsonic or transonic condition, when inlet intensity located in the range of 1% ~ 20%, the surface pressure and the location of shock wave were unaffected by inlet turbulence intensities.

Figure 22 showed surface temperature distributions with various inlet turbulence intensities at the two conditions. For various intensities, the trends of temperature along the surface were consistent, but the temperature values had some difference. With the intensity increasing, surface temperature increased in the region from the stagnation point to 0.43 axial chord on suction side and in the region from the stagnation point to 0.56 axial chord on pressure side. The intensity had insignificant effect on temperature distribution in the latter regions. In the two conditions, the predicted temperature under the low intensity (1%) had a large difference from the one under the medium intensity (6.5%). In the range of intensity 3% ~ 20%, the surface temperature using intensity 6.5% could be predicted well, with the maximum difference 18K. In the range of intensity 6.5% ~ 20%, the surface temperature using intensity 15 % could be predicted well, with the maximum difference 12K. These opinions might only be adequate for the airfoils.

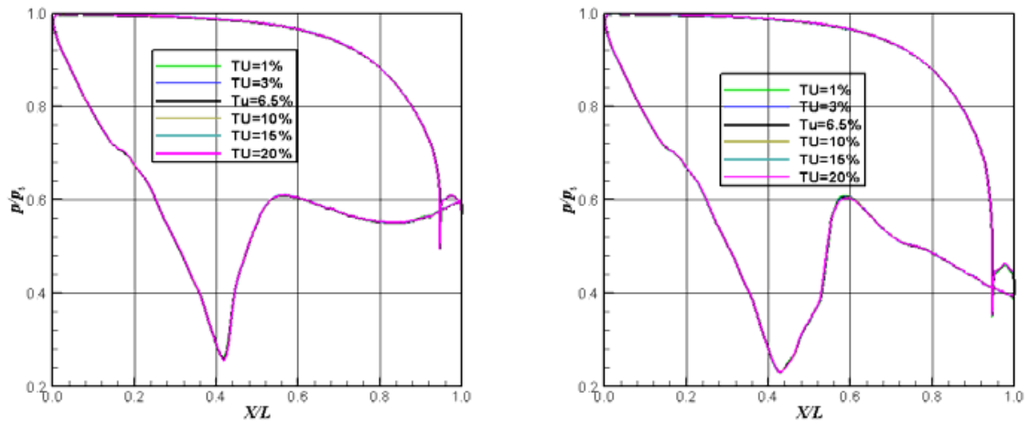

a) Condition 1 b) Condition 2

Fig. 21. Pressure distribution under different inlet turbulence intensities

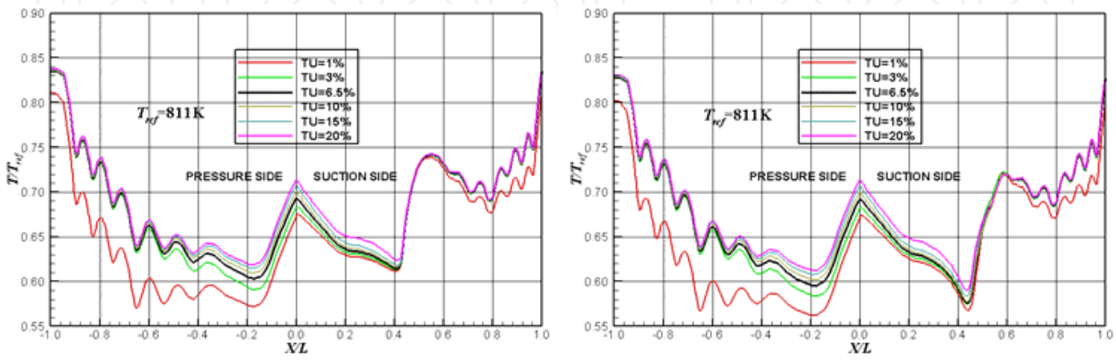

a) Condition 1 b) Condition 2

Fig. 22. Temperature distribution under different inlet turbulence intensities

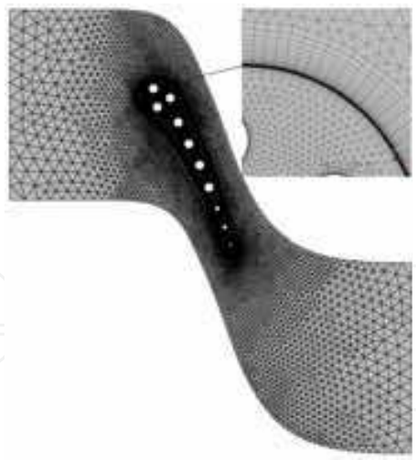

a)

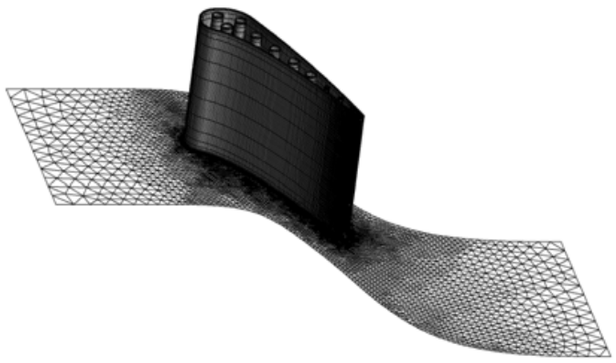

b)

Fig. 23. Computational grid(3D) of MARK Ⅱ cascade

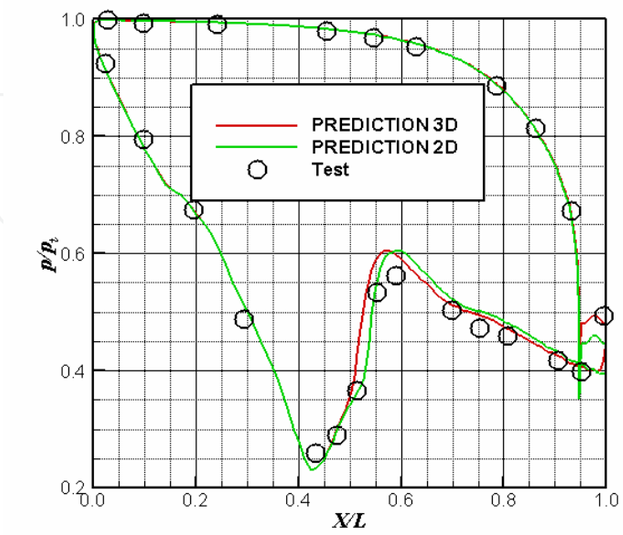

Fig. 24. Pressure distribution (2D and 3D)

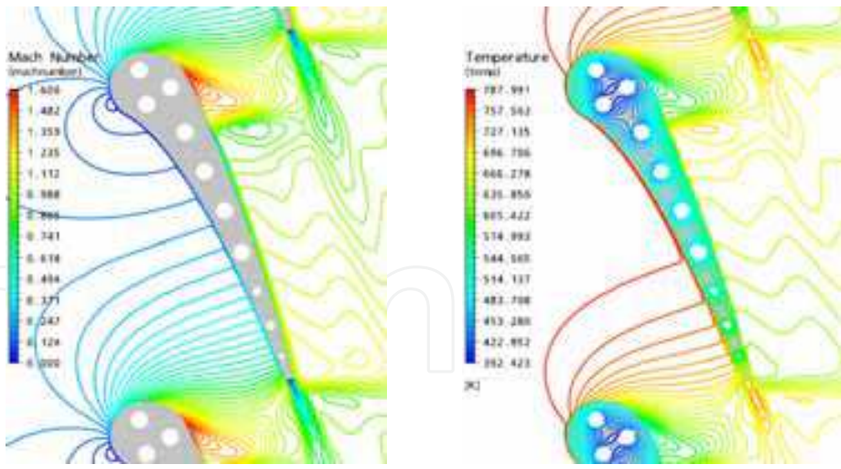

a) 2D simulation

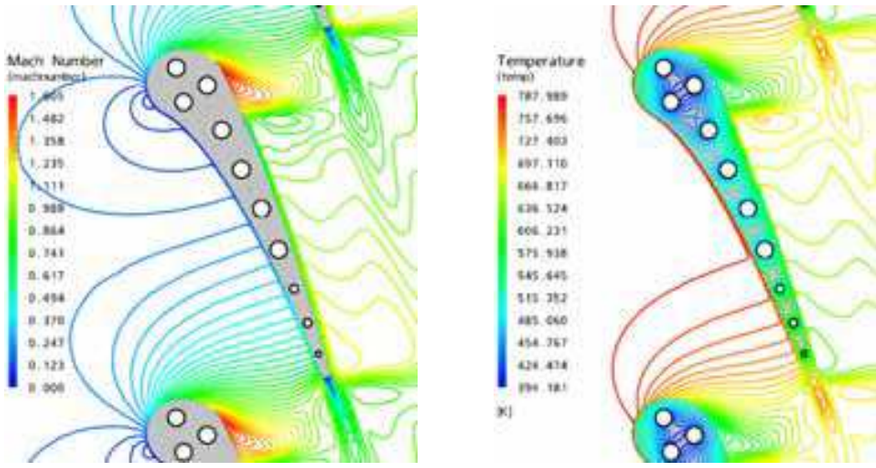

b) 3D simulation

Fig. 25. Contours of Mach Number and Temperature (2D and 3D)

4.2 3D simulation

The 3D simulation used unstructured grid (shown in figure 23), which was got by extruding the 2D grid used in the 2D simulation above. Total number of nodes was 659310 and total number of elements was 788945. Total number of nodes in the fluid domain was 572370 and total number of elements in the fluid domain was 671147. Total number of nodes in the solid domain was 86940 and total number of elements in the solid domain was 117798.

The boundary condition was the same as condition 2 shown in table 3. The boundary conditions of cooling channel were given cooling temperature and heat transfer coefficient, too. The simulation was made using SST turbulence model with transition model. The 3D results on the mean plane were compared to the 2D one.

Figure 24 showed the pressure distribution by using 2D and 3D method. Comparing to 2D result, the location of the end of shock wave was upstream. The reason may be that the endwall had some influence on the flow. The difference between Mach contours were shown in figure 25.

The temperature distribution of 2D and 3D was shown in figure 26 (also can be seen in figure 25). All the results agreed well with the test data, but there were some dissimilarities which may arise from the endwall. The dissimilarities focused on the transition region. For the cascade, the influence of the endwall on the blade surface temperature and HTC distribution could be ignored.

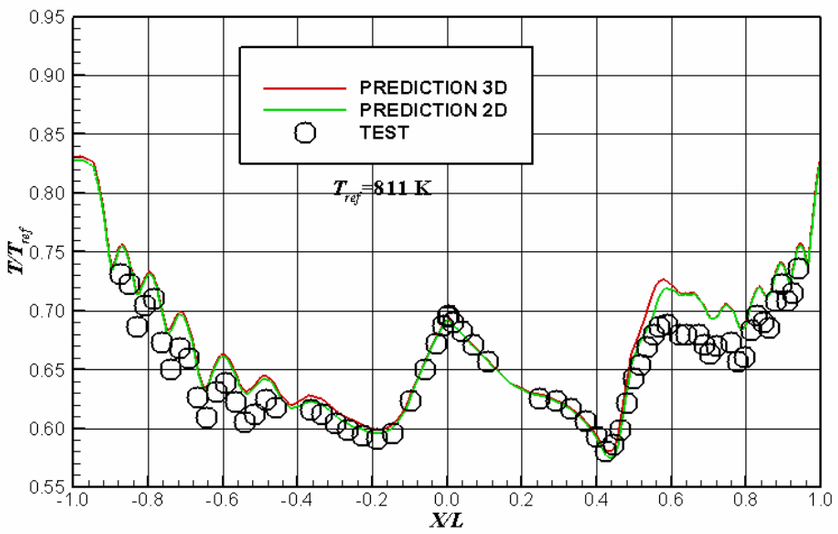

Fig. 26. Temperature distribution (2D and 3D)

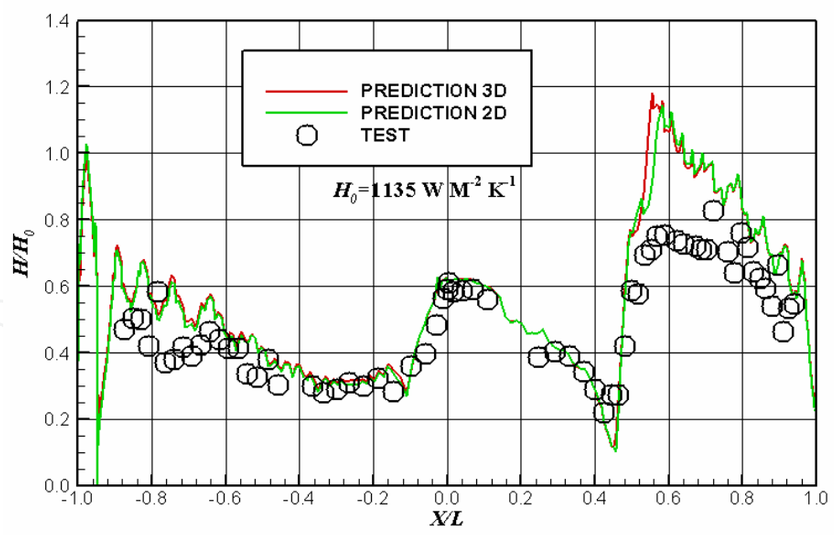

Fig. 27. EHTC distribution (2D and 3D)

5. Conclusion

The 3D method which was used to simulate some cases should be validated. The method calculated URANS equations by employing SST turbulence model with transition model. The cases were T3A flat plate, VKI HPT stator, VKI HPT rotor and Mark II stator. The result

of T3A flat plate showed that the method had high accuracy on predicting flow. All the other results indicated that the method had high accuracy on simulating conjugate flow and heat transfer.

For the conjugate flow and heat transfer problems, two steps were applied. The first step was that no internal cooling cascades, VKI HPT stator and rotor, were calculated. With the good results, the second step was that Mark II stator with internal cooling channel was calculated. Using SST turbulence model with transition model, the accuracy of surface pressure distribution and temperature loading was high. The effect of turbulence models and the one of inlet turbulence intensities were researched, too. The results showed that trend of the temperature along the profile under inlet low turbulence intensity (1%) was different from the one under other intensities. However, there was a shortcoming that the temperature or heat transfer coefficient at the end of the transition region was over predicted results.

For the above simulations, 3D CFD method has high accuracy on predicting conjugate flow and heat transfer problems. But the method should be improved in the transition region.

6. Nomenclature

ρ	Density	kg m^{-3}
U	Velocity	m s^{-1}
t	time	s
x	Cartesian coordinate	m
p	Pressure	kg m^{-1} s^{-2}
μ_{eff}	Effective viscosity	kg m^{-1} s^{-1}
h	Enthalpy	m^2 s^{-2}
T	Temperature	K
c	Solid specific heat	m^2 s^{-2} K^{-1}
λ	Thermal conductivity	kg m s^{-3} K^{-1}
γ	Turbulence intermittency	
μ	Dynamic viscosity	kg m^{-1} s^{-1}
μ_t	Turbulence viscosity	kg m^{-1} s^{-1}
k	Turbulence kinetic energy	m^2 s^{-2}
ω	Turbulence eddy frequency	s^{-1}
Re	Reynolds number	
Tu	Inlet turbulence intensity	
M_2	Exit Mach number	
P_1	Inlet Pressure	kg m^{-1} s^{-2}
T_1	Inlet temperature	K
P_2	Exit Pressure	kg m^{-1} s^{-2}
T_w	Wall temperature	K

subscripts

i,j	Cartesian coordinate

superscripts

*	total

7. References

[1] Mahmoud L. Mansour; Khosro Molla Hosseini & Jong S. Liu. ”Assessment of the impact of laminar-turbulent transition on the accuracy of heat transfer coefficient prediction in high pressure turbines”.ASME GT2006-90273.

[2] Bohn D.; Bonhoff B. & Schonenborn H. ”Combined aerodynamic and thermal analysis of a high-pressure turbine nozzle guide vane”. 95-YOKOHAMA-IGTC-108

[3] Hylton L.D.; Mihelc M.S.; Turner E.R.; Nealy D.A. & York R.E. ”Analytical and experimental evaluation of the heat distribution over the surfaces of turbine vanes”. NASA CR168015, 1983.

[4] Bohn D. & Heuer T. “Conjugate flow and heat transfer calculation of a high pressure turbine nozzle guide vane”. AIAA 2001-3304

[5] Bohn D.; Heuer T. & Kortmann. “Numerical conjugate flow and heat transfer investigation of a transonic convection-cooled turbine guide vane with stress adapted thicknesses of different thermal barrier coatings”. AIAA 2000-1034

[6] Bohn D. & Tümmers C. “Numerical 3-D conjugate flow and heat transfer investigation of a transonic convection-cooled thermal barrier coated turbine guide vane with reduced cooling fluid mass flow”. ASME GT2003-38431

[7] William D.York & James H.Leylek. ”Three-dimensional conjugate heat transfer simulation of an internally-cooled gas turbine vane”.ASME GT2003-38551

[8] Facchini B.; Magi A. & Greco A. S. D. ” Conjugate heat transfer simulation of a radially cooled gas turbine vane”. ASME GT2004-54213

[9] Chunhua Sheng & Qingluan Xue.”Aerothermal analysis of turbine blades using an unstructured flow solver-U^{2}NCLE”.AIAA 2005-4683.

[10] Menter F.R.. ”Two-equation eddy-viscosity turbulence models for engineering applications”. AIAA Journal Vol. 32, No. 8, pp.269-289, 1994.

[11] Menter F.R.; Kuntz M. & Langtry R. ”Ten years of industrial experience with SST turbulence model”.Turbulence Heat and Mass Transfer 4 Begell House Inc., 2003

[12] Menter F.R.; Langtry R.B.; Likki S.R.; Suzen, Y.B.; Huang, P.G. & Völker, S. ”A correlation based transition model using local variables part 1 - model formulation”. ASME GT2004-53452.

[13] Roach, P.E. & Briley, D.H. (1990). “The influence of a turbulent free stream on zero pressure gradient transitional boundary layer development. Part 1: testcases T3A and T3B”. Cambridge University Press.

[14] Tony Arts, “Aero-Thermal Performance of a Two Dimensional Highly Loaded Transonic Turbine Nozzle Guide Vane”, ASME 90-GT-358.

[15] Tony Arts, “External Heat Transfer Study on a HP Turbine Rotor Blade”, Heat Transfer and Cooling in Gas Turbines, AGARD-CP-390: 5-1-5-12.

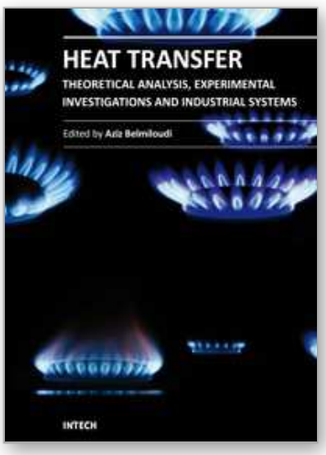

Heat Transfer - Theoretical Analysis, Experimental Investigations and Industrial Systems

Edited by Prof. Aziz Belmiloudi

ISBN 978-953-307-226-5
Hard cover, 654 pages
Publisher InTech
Published online 28, January, 2011
Published in print edition January, 2011

Over the past few decades there has been a prolific increase in research and development in area of heat transfer, heat exchangers and their associated technologies. This book is a collection of current research in the above mentioned areas and discusses experimental, theoretical and calculation approaches and industrial utilizations with modern ideas and methods to study heat transfer for single and multiphase systems. The topics considered include various basic concepts of heat transfer, the fundamental modes of heat transfer (namely conduction, convection and radiation), thermophysical properties, condensation, boiling, freezing, innovative experiments, measurement analysis, theoretical models and simulations, with many real-world problems and important modern applications. The book is divided in four sections : "Heat Transfer in Micro Systems", "Boiling, Freezing and Condensation Heat Transfer", "Heat Transfer and its Assessment", "Heat Transfer Calculations", and each section discusses a wide variety of techniques, methods and applications in accordance with the subjects. The combination of theoretical and experimental investigations with many important practical applications of current interest will make this book of interest to researchers, scientists, engineers and graduate students, who make use of experimental and theoretical investigations, assessment and enhancement techniques in this multidisciplinary field as well as to researchers in mathematical modelling, computer simulations and information sciences, who make use of experimental and theoretical investigations as a means of critical assessment of models and results derived from advanced numerical simulations and improvement of the developed models and numerical methods.

How to reference

In order to correctly reference this scholarly work, feel free to copy and paste the following:

Zeng Jun and Xiongjie Qing (2011). Conjugate Flow and Heat Transfer of Turbine Cascades, Heat Transfer - Theoretical Analysis, Experimental Investigations and Industrial Systems, Prof. Aziz Belmiloudi (Ed.), ISBN: 978-953-307-226-5, InTech, Available from: http://www.intechopen.com/books/heat-transfer-theoretical-analysis-experimental-investigations-and-industrial-systems/conjugate-flow-and-heat-transfer-of-turbine-cascades

INTECH
open science | open minds

InTech Europe
University Campus STeP Ri
Slavka Krautzeka 83/A

InTech China
Unit 405, Office Block, Hotel Equatorial Shanghai
No.65, Yan An Road (West), Shanghai, 200040, China

www.intechopen.com

51000 Rijeka, Croatia
Phone: +385 (51) 770 447
Fax: +385 (51) 686 166
www.intechopen.com

中国上海市延安西路65号上海国际贵都大饭店办公楼405单元
Phone: +86-21-62489820
Fax: +86-21-62489821

IntechOpen

IntechOpen